Lasers in Manufacturing Conference 2023

Investigation on the influence of beam steering frequency on keyhole behavior using a dynamic beam laser

Florian Hugger[a], Robin Sättele[a,*], Jonas Wagner[b], Eric Punzel[a], Andreas Bürger[a]

[a]*BBW Lasertechnik GmbH, Gewerbering 11, Prutting 83134, Germany*
[b]*Institut für Strahlwerkzeuge ISFW, University of Stuttgart, Pfaffenwaldring 43, Stuttgart 70569, Germany*

Abstract

Dynamic beam lasers are the latest tool to influence keyhole behavior in laser welding. Civan's OPA6 laser can change spot position within the working field with a frequency up to MHz range. During these time intervals, the laser beam interacts with the melt at different positions and with rapid position changes. The material surface heats up and cools down in dependence of shape frequency and number of shape points.
A 1D analytical calculation is carried out to determine the influence of different thermal cycles on the surface temperature. From this calculation the time dependent ablation pressure is derived, and the dynamic reaction of the capillary surface is estimated.
This theoretical investigation is compared with experimental results. The behavior of the keyhole surface is analysed by means of high-speed imaging with a frame rate of 400 kHz, applying different beam steering frequencies from 1 kHz to 1,000 kHz.

Keywords: Dynamic beam laser; laser beam welding; keyhole; interaction time

1. Introduction

Dynamic beam lasers are the latest development in beam sources for laser beam welding. Coherent beam combining (CBC) of 32 single mode lasers and optical phased-array (OPA) technologies allow the movement of a main central lobe with gaussian distribution with a point frequency of up to 50 MHz within a matrix (Prieto, 2020; Shekel, 2020). This gives the possibility for quasi-stationary beam profiles to shape keyhole geometry and tailor the temperature field during welding. The more complex the keyhole or temperature field, the more single points must be used to define the beam shape.

For low shape frequencies of 50 Hz the capillary follows the movement of the beam shape, Wagner, 2022. Therefore, the question arises which point frequency is required to reach a "quasi-stationary" capillary,

meaning a capillary wall with no or negligible movement. This paper investigates this question from an experimental and theoretical point of view.

2. Experimental Setup

The influence of dynamic beam shaping on the spatial response of the capillary front is experimentally investigated by means of high-speed imaging. The experiments are conducted with 1mm stainless steel 1.4301 samples in full penetration laser beam welding to minimize the influence of recoil pressure on the capillary surface movement. All experiments are executed with constant laser power $\mathrm{P_L} = 1.8\mathrm{kW}$ and constant feed rate $\mathrm{v_{feed}} = 6\ \mathrm{m/min}$ of the workpiece in positive x-direction (Fig. 1). The length of the weld seam was set to 100 mm. To capture the welding process, two high-speed cameras are set-up according to fig. 1.

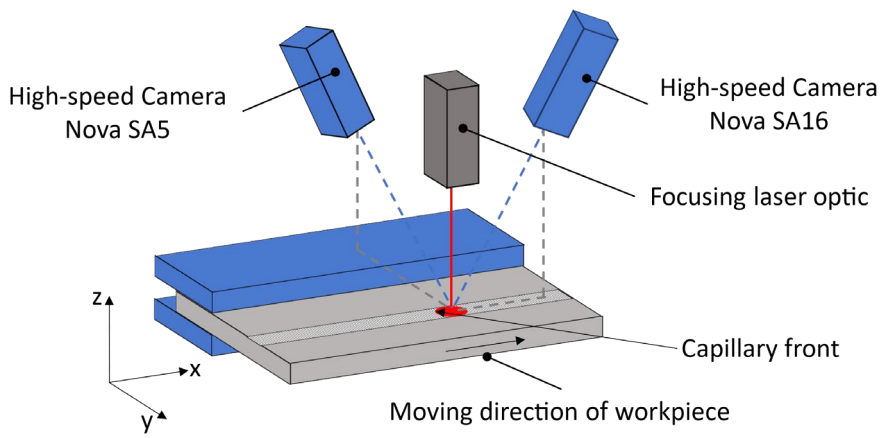

Fig. 1. Experimental setup with work piece, laser beam and two high-speed cameras

$\mathrm{Camera_1}$(Nova SA16) is positioned in lateral direction of the weld seam with an inclination angle of 26.5°, a recording frequency of $\mathrm{f_{Cam1}} = 400\ \mathrm{kHz}$ and a resolution of 128x80px. The pixel to real-world-coordinate ratio is approximately $8.8\mu\mathrm{m/px}$ in x-direction. The camera focus is set to the capillary front at the sample surface. A high-power LED illuminates the capillary at a wavelength of 630nm. A short pass filter in $\mathrm{Camera_1}$ is designed for the wavelengths $615 - 645\mathrm{nm}$. $\mathrm{Camera_2}$ (Nova SA5) is placed in lateral direction of the weld seam with an inclination angle of 30°, a recording rate of 50 kHz and a resolution of 512 x 264 px. The results of $\mathrm{Camera_2}$ are used to validate the results extracted from $\mathrm{Camera_1}$. A bandwidth filter was utilized to only capture the self-illumination of the capillary and cut off the laser beam wavelength as well as the high-power LED. The high-speed cameras are synchronized with the same trigger signal.

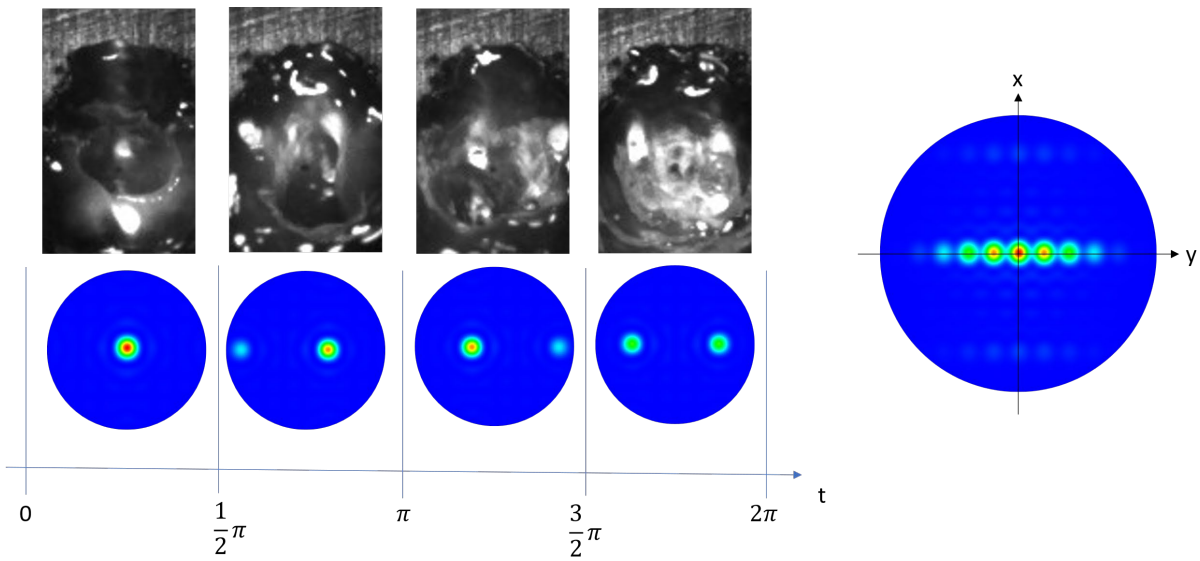

Fig. 2. a) Shape sequence with varying intensity distributions and corresponding images from Camera_1 at 1kHz shape frequency; b) Quasi static beam shape with coordinate system set according to coordinate system from Fig. 1

The OPA6 laser from Civan is used for all samples with a focusing lens having a focal length of $f_l = 1.5\ \mathrm{m}$. The result is a focal spot $d_f = 900\ \mu\mathrm{m}$, whereby each individual spot in the working field has a diameter of $d_{if} = 90\ \mu\mathrm{m}$. For the experiments a shape sequence according to fig. 2 is chosen. A changing intensity distribution perpendicular to the feed direction is applied to the work piece to create a varying intensity distribution in y-direction. Experiments with shape frequencies between $1\mathrm{kHz} < f_{\mathrm{Shape}} < 1{,}000\mathrm{kHz}$ are conducted. The corresponding interaction time for each beam shape within a sequence is four times smaller.

3. Experimental analysis of beam shaping influence on capillary front movement

The recorded high-speed images are analyzed at the center spot of the beam shape in x-direction. Therefore, streak images are generated from the high-speed recordings of camera 1. From each consecutive frame the constant pixel row which corresponds to the center of the beam shape is extracted and stacked horizontally. This results in an image where the vertical axis describes the movement of the capillary front and the horizontal axis the time with the step size $T_{\mathrm{frame}} = 2.5\ \mu\mathrm{s/px}$. The extraction process is visualized in fig. 3. First the streak image is contrast enhanced with the CLAHE-algorithm and $\mathrm{clip}_{\mathrm{limit}} = 2.0$, Bradsky, 2000. Using the known laser and camera frequencies and a starting point the streak image is separated into single shape sequences with image width $w = f_{\mathrm{camera1}} / f_{\mathrm{shape}}$ and height $h = 128$ starting at $t = 0\ \mu\mathrm{s}$. The capillary front movement is determined by thresholding and skeletonizing. This step is executed manually and assisted by the recordings of Camera_2. The capillary movement is analyzed for the first shape in the sequence at the center of the focal spot.

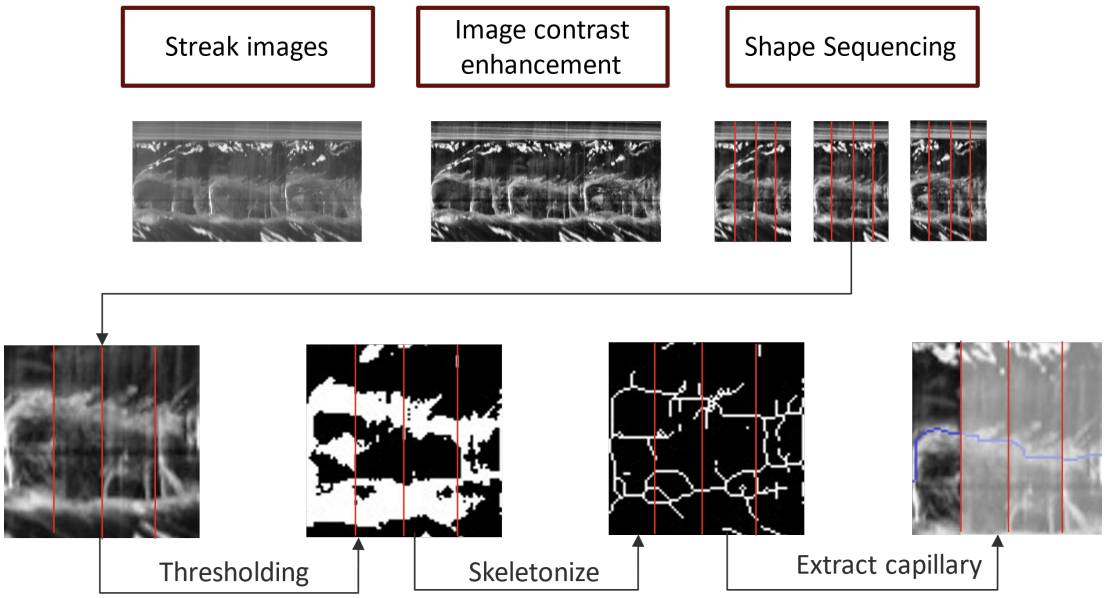

Fig. 3. Generation of streak images and following image processing to retrieve the capillary front.

Due to the high fluctuations of the capillary, induced by an unstable welding process, each shape sequence starting point $x_n[t = 0]$ is set to the last point of the previous sequence $x_{n-1}[t = T_{end}]$. Finally, the mean curve and corresponding standard deviation of all analyzed sequences is calculated.

From the conducted experiments laser frequencies up to 20kHz are analyzed with at least 20 frames per shape sequence. fig. 4 shows the results of the capillary movement extracted from the high-speed recordings. At very low shape frequencies of 1 kHz a large overshoot of the capillary front is detected at 50 µs. During the expansion of the capillary the dynamic pressure p of the capillary is larger than the ambient pressure and the surface tension combined. At 5 0µs this power imbalance is reversed, and the capillary is shrinking towards an equilibrium. The continuously changing intensity profile prevents the capillary to reach the equilibrium and maintains an unstable keyhole with large fluctuations. Increasing the frequency to 5 kHz avoids the overshooting and decreases the fluctuations. Further increasing the point frequency leads to smaller capillary distance movements and smaller standard deviations.

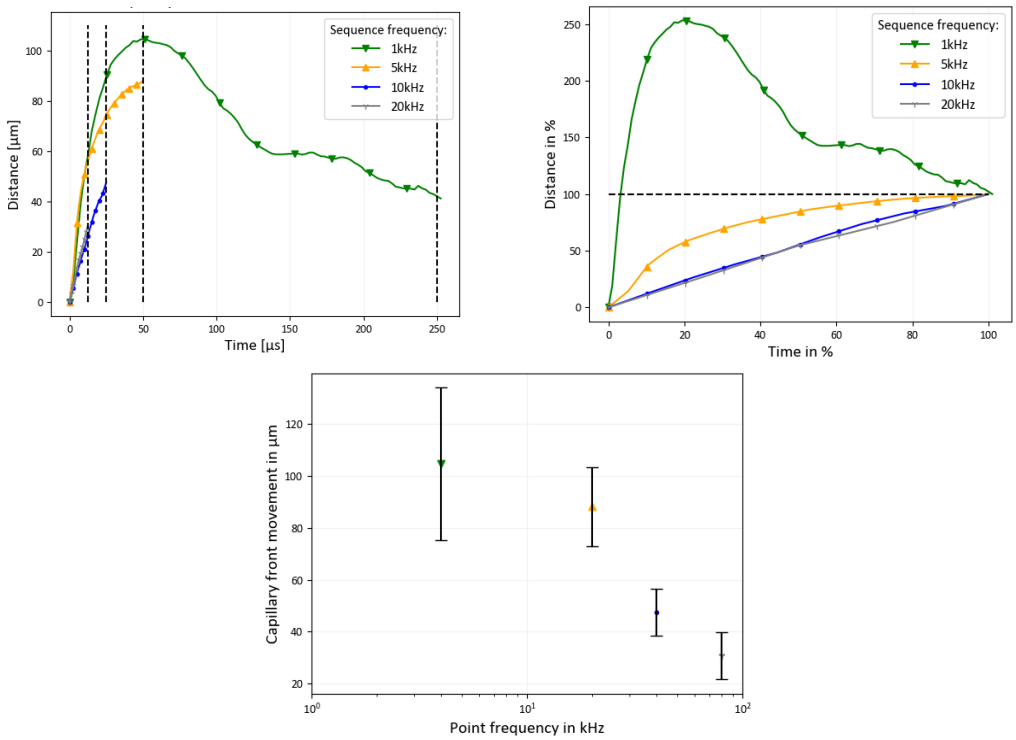

Fig. 4. Results of capillary movement from experiments: a) Absolute values b) normalized values, the distance axis is divided by the last end value of the capillary front while the time axis is stretched to 100% c) influence of point frequency on capillary distance with standard deviation, the distance value is extracted from the peak position of the mean curve.

4. 1D-calculation of capillary movement

The calculation is based on an iteration process beginning with a temperature T. From the temperature an ablation pressure p at the capillary surface is calculated. The ablation pressure p is the input parameter for the calculation of the acceleration a of the capillary front. From the acceleration a new position of the capillary front r at the next time step is derived. The new capillary radius r is the basis for the calculation of the intensity on the surface I, for which a gaussian beam is defined. The side loops are ignored for simplicity. As the last step, the temperature T on the surface is calculated from the intensity I as input for the next iteration loop. In total 100,000 iteration loops were calculated for each parameter setting.

The intensity at the capillary surface I with respect to the capillary radius r is calculated by equation (1), Hügel, 2014, with a laser power P = 5 kW and a beam diameter of r_F = 50 µm.

$$I_L = 2 * \frac{P_L}{\pi * r_F^2} e^{-2*\left(\frac{r}{r_F}\right)^2} \quad (1)$$

From the intensity I the temperature T is calculated applying equation (2), Hügel, 2023.

$$T(t > \tau) = T_0 + \frac{A*I}{\lambda_{TH}} [l_{DIF} * ierf(0) - l^*_{DIF} * ierf(0)] - T^* \quad (2)$$

Here T is the temperature of the capillary surface, t is the time, τ is the interaction time of the laser beam with the capillary front, T_0 is the starting temperature which is set to T_0 = 2,800 K, A is the absorptance which is set to 0.7, I is the intensity, λ_{TH} is the heat conductivity, l_{DIF} and l_{DIF}^* are the diffusion lengths, ierf(0) = 0.56 is the integrated error function at the surface and T^* = 0.3*T_0 is a temperature to estimate heat loss by heat conduction and to avoid heat accumulation when the equation is iterated. l_{DIF} and l_{DIF}^* can be calculated by equations (2) and (3), Hügel, 2023.

$$l_{DIF} = 2 * \sqrt{k * t} \quad (3)$$

$$l_{DIF}^* = 2 * \sqrt{k * (t - \tau)} \quad (4)$$

k=0.000023 m^2/s is the thermal diffusivity and τ is the interaction time of laser beam and surface. The point frequency is 1/τ. The point frequency is always factor 4 of the shape frequency since the shape consists of 4 points.

From the temperature T the pressure p at the capillary surface was calculated applying the Clausius-Clapeyron-equation (5), where p_0 is the ambient pressure, ΔH_V = 347,000 J/mol is the molar enthalpy of evaporation, R_M = 8.314 is the gas constant, T_V =3,134 K, Wolfram Alpha, 2023, is the evaporation temperature at atmospheric pressure and p_{OS} = 35,000 Pa is the pressure due to surface tension with a capillary radius of r_F = 50 µm. An evaporation equilibrium state was assumed and thus no condensation coefficient was considered.

$$p = p_0 * exp\left[\frac{\Delta H_V}{R_M}\left(\frac{1}{T_V} - \frac{1}{T}\right)\right] - p_{OS} \quad (5)$$

Finally, the acceleration a of the capillary surface is a function of the pressure p, and is calculated by equation (6), where ρ=7,800 kg/m^3 is the density of the liquid steel and d = 0.2 mm is the thickness of the melt film between the surface and the solid material.

$$a = \frac{p}{\rho * d} \quad (6)$$

The following picture show the results for capillary movement r, temperature T, pressure p and intensity I for the first t = 500 µs for a point frequency of f = 50 kHz, respectively. The initial values for capillary radius and temperature are r_0 = 45 µm and T_0 = 2,800 K.

The capillary radius r first increases from 45 µm to 56 µm and then stabilizes in an oscillation around 48 µm. Beginning at a temperature of 2,000 K the temperature increases at the beginning and like the capillary radius oscillates from 100 ps on between 2,000 k and 3,700 K. The pressure at the surface shows peaks every time the temperature significantly exceeds the evaporation temperature of the material (Fig. 5). For the intensity at the surface the same behavior is obvious.

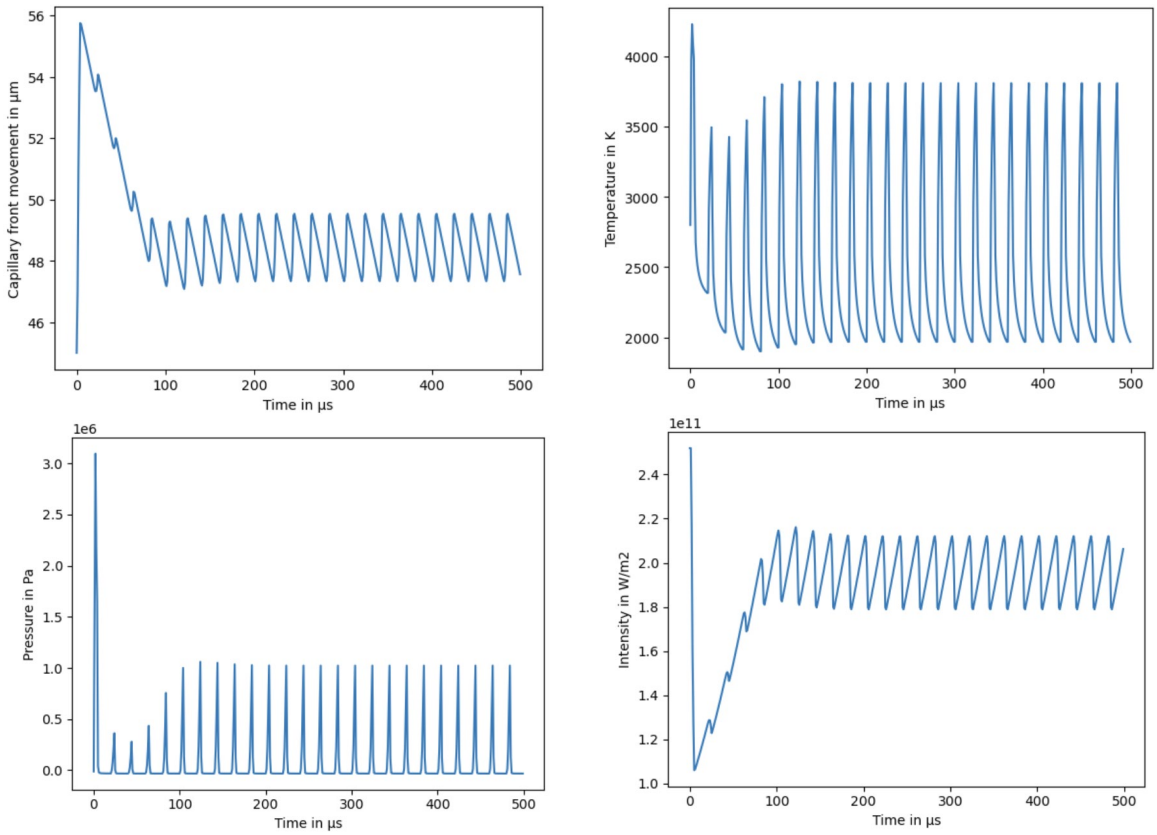

Fig.5. (a) Capillary movement, (b) Temperature, (c) Pressure and (d) Intensity for a point frequency of 50 kHz for the first 500 µs

Calculations with different point frequencies show that the capillary radius r is decreasing with increasing point frequency. This can be drawn to a decreasing peak temperature, and following lower surface pressure, at the capillary surface with increasing frequency due to the shorter interaction time. Moreover, the distance of the oscillation of upper and lower limit of the capillary front is decreasing with increasing frequency. With increasing frequency, the peak temperature T during the interaction time τ is lower and the surface is heated more often which leads to more, but smaller movements of the capillary surface.

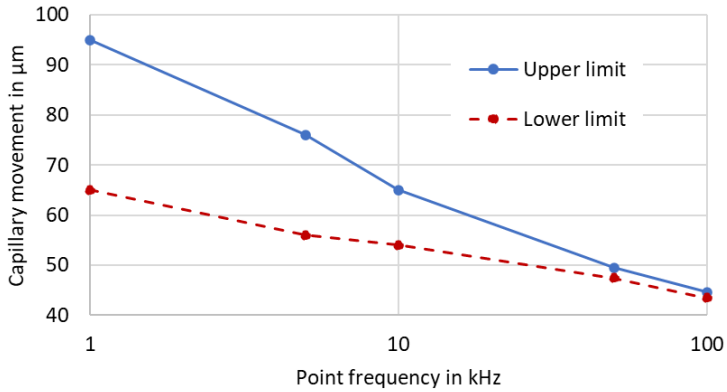

Fig.6. Influence of point frequency on capillary movement distance.

5. Conclusion

The impact of dynamic beam shaping on the oscillation of the capillary surface was investigated for stainless steel 1.4301 in full penetration laser beam welding. Experimental studies and a theoretical 1D calculation were carried out suggesting similar results. Increasing the point frequency leads to smaller capillary movements overall and thus to a more stable keyhole. Furthermore, at very low frequencies it could be shown, that the capillary movement direction reversed before the next shape was active leading to an increased capillary pressure once the next shape starts resulting in an unstable keyhole.

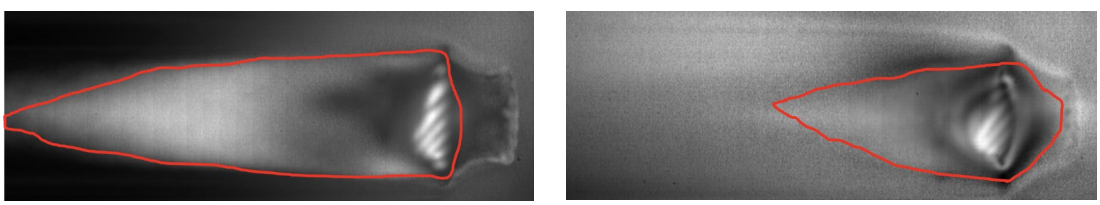

Fig. 7. Plot of calculated standard deviation from high-speed imaging for a) 100 kHz and b) 1,000 kHz shape frequencies. The line marks the melt pool shape.

The high frequency images of 100 kHz and 1,000 kHz show a change of the capillary shape and the melt flow. Therefore, the standard deviation of each video is plotted in fig. 7. Bright areas show high turbulences from increased melt flows and surface movement. The red line marks the melt pool. The experiment with 100 kHz has a strong melt flow to the back of the weld seam leading to an extended melt pool behind the capillary. The dark area to the backside of the capillary is a constant upstream of melt forming a continuous hump. The experiment with 1,000 kHz sequence frequency has a shorter melt pool to the back of the capillary but a bigger melt pool in the front of the capillary compared to the experiment with 100 kHz. These results suggest there is further investigations to be done to understand the interaction between dynamic beam shaping and the capillary.

Acknowledgements

We thank the IFSW Stuttgart to conduct the experiments at their facilities and for providing Civans OPA6 laser system and the Nova SA5 high-speed camera.

References

Bradski, G., 2000. The OpenCV Library. Dr. Dobb's Journal of Software Tools.

Hügel, H, Graf, T, 2014. Laser in der Fertigung. Grundlagen der Strahlquellen, Systeme, Fertigungsverfahren, 3. Auflage.

Hügel, H, Graf, T, 2023. Materialbearbeitung mit Laser, 5. Auflage.

Prieto, C., Vaamonde, E., Diego-Vallejo, D., Jimenez, J., Urbach, B., Vidne, Y., Shekel, E., 2020. Dynamic laser beam shaping for laser aluminium welding in e-mobility applications. 11th CIRP Conference on Photinic Technologies [LANE 2020].

Shekel, E., Vidne, Y., Urbach, B., 2020. 16kW single mode CW laser with dynamic beam for material processing. Proceedings Volume 11260, Fiber Lasers XVII: Technology and Systems; 1126021 [SPIE LASE 2020]

Wagner, J. et al., 2022, Influence of dynamic beam shaping on the geometry of the keyhole during laser beam welding. Procedia CIRP. 111. 448-452. 10.1016/j.procir.2022.08.185.

Wolfram Alpha LLC: Wolfram Alpha 2023